Melting, Bubblelike Expansion, and Explosion of Superheated Plasmonic Nanoparticles

Simon Dold,[1,2,*] Thomas Reichenbach,[3,*] Alessandro Colombo,[4,*] Jakob Jordan,[5] Ingo Barke,[6,7] Patrick Behrens,[5] Nils Bernhardt,[5] Jonathan Correa,[8] Stefan Düsterer,[8] Benjamin Erk,[8] Thomas Fennel,[6,7] Linos Hecht,[4] Andrea Heilrath,[5] Robert Irsig,[6] Norman Iwe,[6] Patrice Kolb,[4] Björn Kruse,[6] Bruno Langbehn,[5] Bastian Manschwetus,[8] Philipp Marienhagen,[9] Franklin Martinez,[6] Karl-Heinz Meiwes-Broer,[6,7] Kevin Oldenburg,[6,7] Christopher Passow,[8] Christian Peltz,[6] Mario Sauppe,[4,5] Fabian Seel,[5] Rico Mayro P. Tanyag,[5] Rolf Treusch,[8] Anatoli Ulmer,[5,10] Saida Walz,[5] Michael Moseler,[1,3] Thomas Möller,[5] Daniela Rupp,[4,11,†] and Bernd von Issendorff[1,12,‡]

[1]*Institute of Physics, University of Freiburg, Hermann-Herder-Straße 3, 79104 Freiburg, Germany*
[2]*European XFEL GmbH, Holzkoppel 4, 22869 Schenefeld, Germany*
[3]*Fraunhofer IWM, MikroTribologie Centrum μTC, Wöhlerstraße 11, 79108 Freiburg, Germany*
[4]*Laboratory for Solid State Physics, ETH Zurich, 8093 Zurich, Switzerland*
[5]*Institut für Optik und Atomare Physik, Technische Universität Berlin, Hardenbergstraße 36, 10623 Berlin, Germany*
[6]*Institute of Physics, University of Rostock, Albert-Einstein-Straße 23-24, 18059 Rostock, Germany*
[7]*Department Life, Light and Matter, University of Rostock, Albert-Einstein-Straße 25, 18059 Rostock, Germany*
[8]*Deutsches Elektronen-Synchrotron DESY, Notkestr. 85, 22607 Hamburg, Germany*
[9]*Institute of Chemistry, University of Rostock, Albert-Einstein-Straße 3a, 18059 Rostock, Germany*
[10]*Department of Physics, Universität Hamburg, Luruper Chaussee 149, 22761 Hamburg, Germany*
[11]*Max Born Institute for Nonlinear Optics and Short Pulse Spectroscopy, 12489 Berlin, Germany*
[12]*Freiburg Materials Research Center, Universität Freiburg, Stefan-Meier-Straße 21, 79104 Freiburg, Germany*

(Received 31 August 2023; revised 8 April 2024; accepted 14 February 2025; published 3 April 2025)

We report on time-resolved coherent diffraction imaging of gas-phase silver nanoparticles, strongly heated via their plasmon resonance. The x-ray diffraction images reveal a broad range of phenomena for different excitation strengths, from simple melting over strong cavitation to explosive disintegration. Molecular dynamics simulations fully reproduce this behavior and show that the heating induces rather similar trajectories through the phase diagram in all cases, with the very different outcomes resulting solely from whether and where the stability limit of the metastable superheated liquid is crossed.

DOI: 10.1103/PhysRevLett.134.136101

Condensed matter, when heated slowly, undergoes the familiar phase transitions from solid to liquid to gas. Extremely fast heating, on the other hand, results in additional phenomena, such as strong overheating of solids or liquids or even a change in the chemical bonding itself due to strongly excited electrons [1–4]. Many aspects of matter under such extreme conditions, like the coupling between a very hot electron gas and the ionic system, are not yet fully understood [5,6]. Isolated nanoscale particles have been identified as well-controlled test objects for the study of highly excited matter [7–9], especially in combination with single-shot coherent diffraction imaging (CDI) using intense x-ray free-electron laser pulses [10–14], which permits one to follow the dynamics with high spatiotemporal resolution [15]. Up to now, most time-resolved studies concentrated on rare gas particles in free flight, excited by strong laser fields [9,15–18], and a few other systems like silicon dioxide particles [19]. Time-resolved diffraction studies on metal nanoparticles were mainly performed using particles supported on surfaces, leading to the observation of vibrational excitation, melting, or disintegration [20–27]. However, an unambiguous analysis of the particle dynamics free from the hard to quantify influence of the support is only possible in the gas phase.

In this Letter, we study silver nanoparticles heated in free flight by excitation of their plasmon resonance with moderately intense picosecond laser pulses. Such particles have been shown to form well-defined faceted crystalline structures at lower temperatures [28–30], distinctly different from the round shape of a liquid droplet, which should facilitate the observation of melting. Furthermore, they exhibit a strong Mie plasmon resonance in the near

*These authors contributed equally to this work.
†Contact author: ruppda@phys.ethz.ch
‡Contact author: bernd.von.issendorff@uni-freiburg.de

UV [31,32], which permits to excite them using fairly weak laser fields [32–36]. This excitation leads to a rather uniform heating of the particle via very fast formation of a hot electron gas and a subsequent transfer of the energy to the nuclear degrees of freedom on a timescale of several picoseconds [36–41]. Employing pump-probe CDI, we determine the morphology of the particles as a function of delay time. Accompanying molecular dynamics simulations of the process provide comprehensive insight into the origin of the observed phenomena. The strength of a decompression wave following the initially isochoric heating of the particles turns out to be a decisive parameter for the dynamics.

The experiment was performed at the free-electron laser (FEL) FLASH [42] using the CAMP end-station [43]. Silver nanoparticles with diameters in the range of 50–200 nm were produced by a magnetron sputter gas aggregation source [44–46], operated with a mixture of xenon and argon. The beam of neutral nanoparticles traversed a differential pumping stage before entering the main chamber. Here, the particles were intercepted by 20 μJ FEL pulses with about 70 fs pulse duration at 5.1 nm wavelength, focused to a spot size of 10 μm. Photons scattered from the particles were collected by a pnCCD detector [47] at a distance of 70 mm from the interaction region at a repetition rate of 10 Hz. Heating of the particles was achieved by 400 nm laser pulses synchronized with the FEL pulses and overlaid in a near-collinear geometry. They were produced by a frequency doubled Ti:Sapphire femtosecond laser system and stretched to a duration of about 1 ps by propagation through 100 mm of fused silica. We note that due to the timescale of the electron-phonon heat transfer of several picoseconds, shorter pulses would not increase the temporal resolution but would just lead to unwanted strong field effects. The 50 μJ pulses were weakly focused to a spot size of roughly 70 μm diameter in the interaction region. Inhomogeneities in the laser beam profile did not permit a precise UV laser intensity determination; we estimate a maximal value of 1×10^{12} W/cm^2, but most of the particles will have experienced lower intensities.

In Figs. 1(a)–1(e) examples of scattering images recorded with the pump pulse present are shown, along with real-space reconstructions obtained by iterative phase retrieval reconstruction [48–51] of the small angle part of the images [30]. These can be interpreted as projections of the particle densities onto a plane perpendicular to the x-ray beam (see Supplemental Material [52] for details). Five different classes can be identified, based on the real-space features of the samples. The *faceted* class in Fig. 1(a) contains polyhedra with well-defined facets, which appear not to be strongly affected by the pump laser, either because the images were recorded at negative or small positive delay times, or because the particles have interacted only with a low-intensity part of the pump laser profile. Figure 1(b) represents examples of the *round* class; these are mostly spherical particles with homogeneous density,

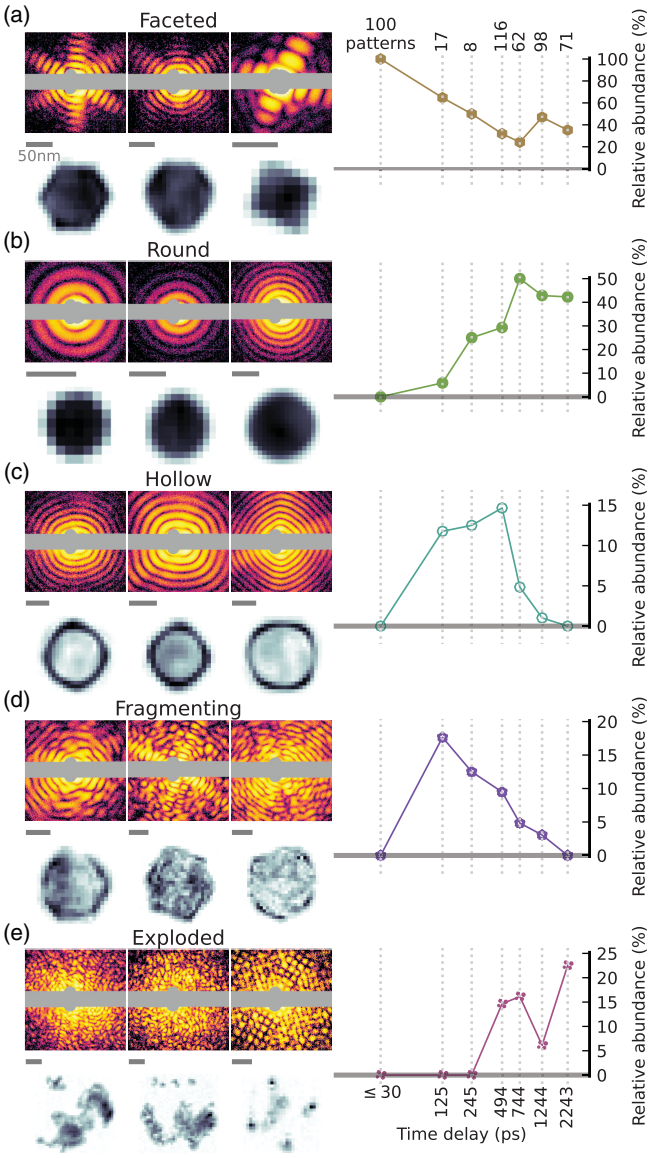

FIG. 1. Characteristic classes of images. Three examples are provided for each class, with the experimental diffraction patterns in logarithmic color scale and the corresponding reconstructions in linear gray scale (object sizes indicated by 50 nm bars). In the right column, respective relative abundances of each class as function of the time-delay between pump laser and FEL pulses are given, with the absolute number of patterns at each delay at the top.

most probably liquid droplets melted due to the heating. Figure 1(c) shows the most spectacular class, *hollow* particles with a rounded outer surface and a large, close to spherical cavity inside. In some cases, the remaining shell has a thickness of only about 10% of its diameter. The *fragmenting* class [Fig. 1(d)] refers to particles with a very inhomogeneous density, indicating disintegration probably due to fairly strong excitation. The *exploded* class [Fig. 1(e)] includes all patterns that correspond to unconnected fragments of the original particle, which leads to specklelike diffraction patterns. These obviously are

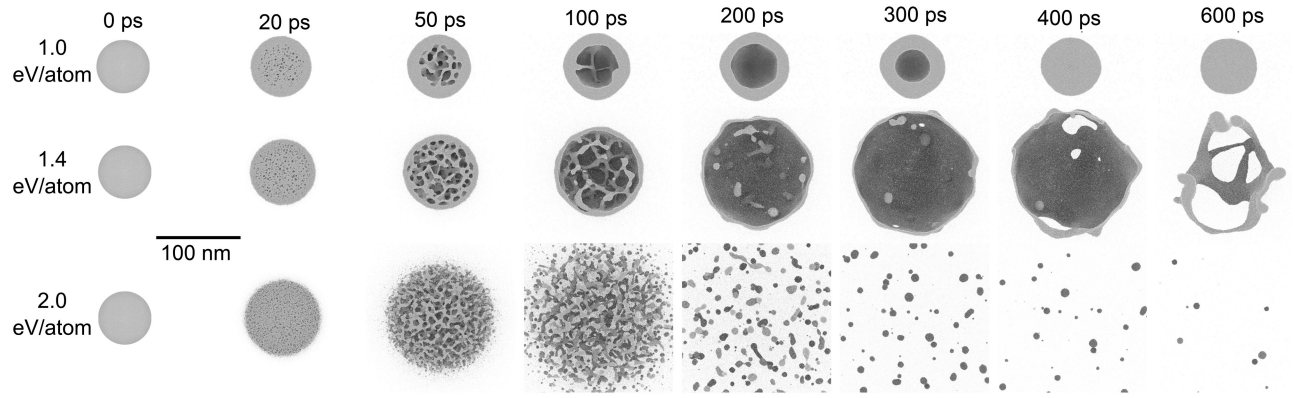

FIG. 2. MD simulations of strongly heated silver particles with 8×10^6 atoms. The snapshots show sectional views for different times, for three different amounts of deposited energy. See Supplemental Material [52] for videos of the dynamics.

particles which completely disintegrated after the interaction with the pump laser. Interestingly, rather symmetric speckle patterns are sometimes observed (like in the third image in this row), corresponding to a small number of large fragments in a rather regular arrangement.

The relative abundances of these five classes as a function of the time delay between the pump laser and the FEL pulse are plotted in the right column of Fig. 1. The total number of identifiable diffraction images recorded at each time delay is given on the top, showing the overall low hit rate in this experiment. For negative and small positive time delays up to 30 ps (here grouped together in a single data point) only faceted structures were observed. Other morphologies start to appear at a delay of 125 ps. The abundance of *faceted* samples drops to a level of about 40% within the first few hundreds of picoseconds. The abundance of *round* specimens exhibits the opposite behavior, rising up to 40% in the first few hundreds of picoseconds. *Exploded* patterns appear even later, at around 500 ps, and tend to become more and more abundant toward longer time delays. The other two classes appear only transiently. The contribution of the *fragmenting* class is significant only between 125 ps and 744 ps; a similar behavior is seen for the *hollow* class, with the maximum abundance apparently shifted to slightly longer delays.

In order to better understand the observed dynamics, the temporal evolution of strongly heated silver particles was simulated by classical molecular dynamics (MD), employing the embedded-atom-method interaction potential of Sheng *et al.* [53]. Experimental diffraction data on pristine samples reveal diverse geometries of the particles [as shown in Fig. 1(a) and discussed in Ref. [30]]. For simplicity, we discuss here the case of spherical particles ($R = 31$ nm, 8×10^6 atoms); faceted shapes lead to qualitatively very similar results (see Supplemental Material [52]). To mimic the heating process by electron-phonon coupling, the particles were thermalized for a duration of 10 ps using a Langevin thermostat with a given temperature in a range between 2000 K and 9000 K, using a relaxation time of 5 ps (see Supplemental Material [52] for details and for a discussion on the influence of the energy deposition method). The total amount of energy deposited into the particles in this way ranges from 0.5 to 2.0 eV/atom. Results of the MD simulations for three cases are shown in Fig. 2. Snapshots of the nanoparticles are depicted at different times after the start of the heating process. In the Supplemental Material [52], videos of the dynamics are provided. In general, the simulation results are in line with those of earlier studies [26,54,75–79]. In the case of a deposited energy of 1.0 eV/atom (first row), small voids start to form in the inner part of the sphere briefly before 20 ps. These voids grow and coalesce into a single large cavity in the center of the particle within 200 ps. This central cavity then contracts again, leading to a round liquid droplet at a delay time of 400 ps. For an energy of 1.4 eV/atom (second row), the initial behavior is similar, but the void formation now happens even closer to the particle surface. As before, the voids merge to form a single central cavity within 200 ps but with a substantially thinner outer shell. In this case, the surface tension is not strong enough to reverse the expansion of the bubble; it further expands and bursts in less than a nanosecond, forming rather large, initially tubular and eventually round fragments. The last case represents the dynamics of the system for a deposited energy of 2.0 eV/atom. Here, the formation of voids happens in the whole volume, even at the surface of the sample. This leads to a direct and violent disintegration of the sample within the first 100 ps, with fragments spreading at significant velocities.

These results are in good agreement with the experimentally observed time evolution (Fig. 1). As mentioned, the *faceted* particles surviving up to long time delays [Fig. 1(a)] most probably have only weakly interacted with the pump laser. The appearance of round droplets around 500 ps is compatible with still rather weakly excited particles, which just melt, or with slightly more strongly excited ones, where a central cavity appears and vanishes again, as in the simulation for a deposited energy of

1.0 eV/atom (Fig. 2). The observation of large bubbles only between 125 ps and 744 ps is congruent with the simulations with both 1.0 eV/atom and 1.4 eV/atom, where the bubble vanishes again at larger times, either by contraction or by fragmentation. The rapid increase of *fragmenting* samples already at 125 ps can be assigned to early, fairly violent void formation, somewhere between the behavior simulated for 1.0 eV/atom and 1.4 eV/atom. The still significant presence of these samples up to around 1 ns hints at processes more in line with the 1.4 eV/atom simulation, indicating bursting bubbles. Finally, the *exploded* samples can stem as well either from early violent fragmentation or a late bursting of a bubble; especially the third example in Fig. 1(e) hints at such a case, because of the small number of larger fragments detected. The square arrangement of the fragments furthermore indicates a fourfold symmetry axis of the initial shape of this particle, as present, e.g., in truncated octahedra [52]. When comparing measured and simulated time dependencies, one should keep in mind that the size of the particles in the simulation is on the lower end of the size distribution of particles observed in the experiment; for the larger particles the dynamics can be expected to be slower than in the simulation.

The question arises why the single large cavity is always formed at the center of the particle. This can be understood with the help of the simulation results, as shown in Fig. 3. Rapid uniform heating of a particle leads to the buildup of a high pressure, which will eventually lead to an overall expansion of the particle. This expansion, however, does not occur via a simple breathing mode motion, but instead in form of a decompression wave: as an acceleration of the material requires a pressure gradient, the motion starts at the particle surface, with the boundary between moving material and material at rest propagating into the particle with the velocity of sound [26,75,80,81]. Figure 3(a) shows the pressure within the particle during the heating phase and the following 10 ps as a function of radial position for the case of an energy deposition of 1.2 eV/atom. One can see that a pressure of more than 20 GPa is reached in the particle center after 6 ps of heating. The motion of the material sets in immediately when the heating is started, with the boundary between moving and nonmoving layers propagating toward the particle center. The position of this boundary is indicated by the black line in Fig. 3(a) (see Supplemental Material for radial profiles of the velocity distributions [52]). It reaches the particle center at about 7 ps, which gives a velocity of sound of about 4400 m/s under these conditions, slightly higher than the room temperature value of 3650 m/s [82]. When this happens, all of the atoms are moving outward, which leads to a strong pressure drop within the particle. This pressure drop is slightly less abrupt than might be expected due to the heating continuing until 10 ps; nevertheless, 14 ps after the start of the heating, a negative pressure of about −2.5 GPa

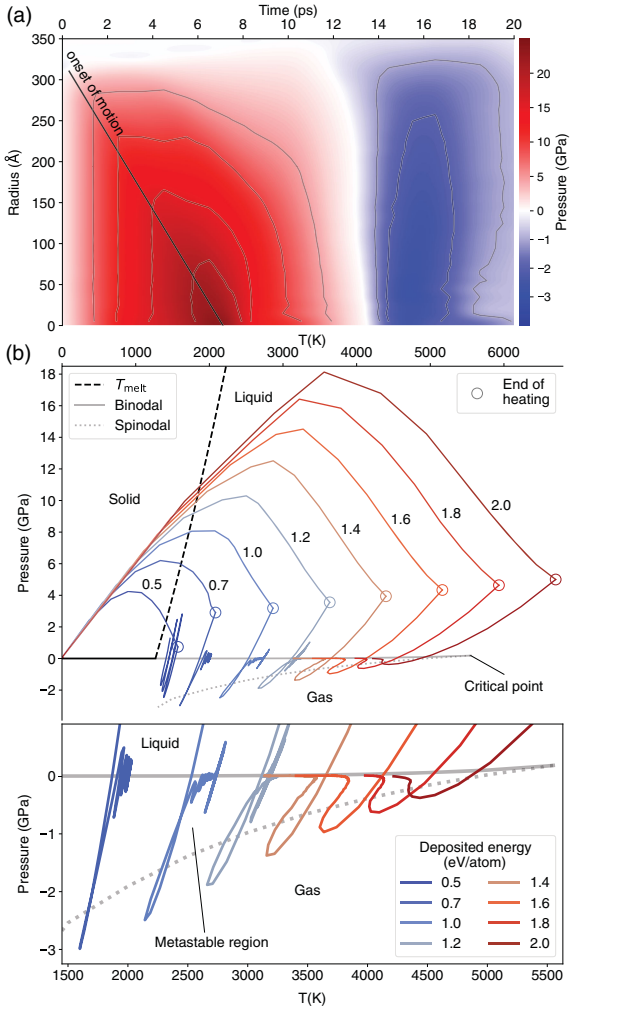

FIG. 3. Evaluation of molecular dynamics simulations. (a) Radial pressure distribution at different times, for an energy deposition of 1.2 eV/atom. The solid line indicates the propagating boundary between material at rest and in motion. (b) Evolution of the system within the phase diagram of silver; the circles indicate the end of the heating process at 10 ps. A detailed view of the metastable region is given in the inset plot below.

is reached [Fig. 3(a)]. As further discussed below, at such a negative pressure cavitation sets in immediately, leading to the many voids as seen in Fig. 2 at 20 ps for 1.0 eV/atom and 1.4 eV/atom. The voids grow and merge into a larger cavity, surrounded by material which continues to move outward as it keeps the momentum gained in the first phase of the expansion. We want to stress that it is not the vapor pressure which drives the growing of this bubble, but rather the outward movement of its shell. Therefore, if this motion is not too fast, it can be reversed by surface tension, as in the 1.0 eV/atom case where the large central void starts to shrink again at about 200 ps and has completely vanished at 400 ps. For higher energy depositions, the initial shell velocity is so high that the surface tension could reverse the motion only at much later stages of the expansion. Before that happens, however, any small hole formed in

the thinning liquid layer leads to the rupture of the bubble [83,84].

At even higher heat bath temperature the particle rips apart immediately. Nevertheless, the underlying mechanism is quite similar to the case of the cavitation process discussed before, as can be best seen by comparing the system trajectories through the phase diagram of silver as shown in Fig. 3(b). In Fig. 3(b) the state of silver is shown as a function of pressure and temperature, with the region most relevant for the experiment magnified. This phase diagram has been obtained from bulk silver MD simulations using the same interaction potential as for the silver particle simulations (see Supplemental Material [52]). In it, the liquid and gaseous region are separated by the so-called binodal, which toward higher temperatures ends in the critical point. Below the binodal, matter should always be in the gaseous state. Nevertheless, the phase transition here is kinetically hindered by seed bubble formation; there is a critical bubble size, which has to be overcome, and which increases the closer the system is to the binodal. Only at a second boundary, the so-called spinodal, the liquid becomes unstable and homogeneous evaporation sets in [26,80,85]. Thus, in the region between the binodal and the spinodal, the liquid can be overheated, staying in a metastable liquid state, while this is not possible anymore beyond the spinodal.

The temporal evolution of the volume-averaged temperature and pressure within the particles is indicated for eight different values of deposited energy (see Supplemental Material [52] for similar phase diagram trajectories calculated for specific radial regions of the particle). Upon heating, one can observe a strong initial increase of temperature and pressure. This in fact moves the system away from the liquid-gas boundary, therefore somewhat stabilizing the liquid. Due to the particle expansion, the pressure drops again despite ongoing heating. Since the energy deposition ends abruptly at 10 ps, which is indicated by the circles, the phase trajectories show an unphysical sharp kink—a more realistic simulation would show a smooth bend instead. Here the temperature starts to drop as well and the systems dive through the binodal. Cavitation, however, sets in only when the systems cross the spinodal, which for the lower temperatures happens at significantly negative pressures. This process is very similar for all heating temperatures; what makes a difference for the highest energy depositions is that here the spinodal is crossed at only slightly negative pressures. Therefore, even after expansion, the system stays close to the spinodal and rupturing continues until total disintegration is reached. One can also observe that for the lowest deposited energy (0.5 eV/atom) the system does not reach the spinodal; in this case no void formation sets in. Instead, the still partly crystalline droplet exhibits a significant breathing mode vibration, a motion strongly damped by the void formation for the next three higher energy deposition cases which end up in compact liquid droplets. Here, however, some breathing mode vibration is excited by the collapse of the cavity, most notably in the 1.2 eV/atom case.

In conclusion, we have demonstrated that the dynamics of strongly heated silver nanoparticles is dominated by a decompression wave caused by the near-isochoric heating, leading to distinct temperature- and time-dependent effects. These sensitively depend on the strength of the electron-phonon coupling and the resulting heating rate of the ions, which opens a new approach to measure the coupling strength up to very high temperatures. From future precision measurements of the onset of cavitation and the time dependence of the expansion and collapse of the bubble, material parameters like the velocity of sound, surface tension, and viscosity under these extreme conditions will also be obtained. Time-resolved x-ray diffraction experiments on nanoparticles in the gas phase are therefore ideally suited to study superheated matter with high spatial and temporal resolution.

Acknowledgments—We acknowledge DESY (Hamburg, Germany), a member of the Helmholtz Association HGF, for the provision of experimental facilities. Parts of this research were carried out at FLASH. Beamtime was allocated for proposal F-20170541. This research was supported in part through the Maxwell computational resources operated at Deutsches Elektronen-Synchrotron DESY, Hamburg, Germany. We acknowledge the Max Planck Society for funding the development and the initial operation of the CAMP end-station within the Max Planck Advanced Study Group at CFEL and for providing this equipment for CAMP@FLASH. The installation of CAMP@FLASH was partially funded by BMBF Grant No. 05K10KT2, No. 05K13KT2, No. 05K16KT3, and No. 05K10KTB from FSP-302. T. M. and B. v. I. acknowledge funding by a DFG Koselleck Project No. MO 719/13 and IS61/14. I. B., T. F., and C. P. acknowledge funding by the Deutsche Forschungsgemeinschaft via SFB 1477 (ID: 441234705). A. C., L. H., M. S., and D. R. acknowledge funding from the Leibniz Society, Germany, via Grant No. SAW/2017/MBI4 and from SNF, Switzerland, via Grant No. 200021E/193642 and the NCCR MUST. T. R. and M. M. acknowledge the Gauss Centre for Supercomputing e.V. for providing computing time on the GCS Supercomputer JUWELS [86] at Jülich Supercomputing Centre. Additional computing time was granted by the state of Baden-Württemberg through bwHPC and the DFG through Grant No. INST39/961-1 FUGG (bwForCluster NEMO).

[1] V. Recoules, J. Clérouin, G. Zérah, P. M. Anglade, and S. Mazevet, Phys. Rev. Lett. **96**, 055503 (2006).
[2] A. M. Lindenberg *et al.*, Science **308**, 392 (2005).
[3] R. Ernstorfer, M. Harb, C. T. Hebeisen, G. Sciaini, T. Dartigalongue, and R. D. Miller, Science **323**, 1033 (2009).

[4] N. Medvedev and I. Milov, Sci. Rep. **10**, 12775 (2020).
[5] M. Mo, Z. Chen, and S. Glenzer, MRS Bull. **46**, 694 (2021).
[6] J.-W. Lee, M. Kim, G. Kang, S. M. Vinko, L. Bae, M. S. Cho, H.-K. Chung, M. Kim, S. Kwon, G. Lee, C. H. Nam, S. H. Park, J. H. Sohn, S. H. Yang, U. Zastrau, and B. I. Cho, Phys. Rev. Lett. **127**, 175003 (2021).
[7] U. Saalmann, C. Siedschlag, and J. Rost, J. Phys. B **39**, R39 (2006).
[8] T. Fennel, K.-H. Meiwes-Broer, J. Tiggesbäumker, P.-G. Reinhard, P. M. Dinh, and E. Suraud, Rev. Mod. Phys. **82**, 1793 (2010).
[9] T. Nishiyama *et al.*, Phys. Rev. Lett. **123**, 123201 (2019).
[10] R. Neutze and K. Moffat, Curr. Opin. Struct. Biol. **22**, 651 (2012).
[11] S. Marchesini, H. N. Chapman, S. P. Hau-Riege, R. A. London, A. Szoke, H. He, M. R. Howells, H. Padmore, R. Rosen, J. C. H. Spence, and U. Weierstall, Opt. Express **11**, 2344 (2003).
[12] K. S. Raines, S. Salha, R. L. Sandberg, H. Jiang, J. A. Rodríguez, B. P. Fahimian, H. C. Kapteyn, J. Du, and J. Miao, Nature (London) **463**, 214 (2010).
[13] N. D. Loh *et al.*, Nature (London) **486**, 513 (2012).
[14] C. Bostedt, E. Eremina, D. Rupp, M. Adolph, H. Thomas, M. Hoener, A. R. B. de Castro, J. Tiggesbäumker, K.-H. Meiwes-Broer, T. Laarmann, H. Wabnitz, E. Plönjes, R. Treusch, J. R. Schneider, and T. Möller, Phys. Rev. Lett. **108**, 093401 (2012).
[15] T. Gorkhover *et al.*, Nat. Photonics **10**, 93 (2016).
[16] L. Flückiger, D. Rupp, M. Adolph, T. Gorkhover, M. Krikunova, M. Müller, T. Oelze, Y. Ovcharenko, M. Sauppe, S. Schorb, C. Bostedt, S. Düsterer, M. Harmand, H. Redlin, R. Treusch, and T. Möller, New J. Phys. **18**, 043017 (2016).
[17] C. Bacellar, A. S. Chatterley, F. Lackner, C. D. Pemmaraju, R. M. P. Tanyag, D. Verma, C. Bernando, S. M. O. O'Connell, M. Bucher, K. R. Ferguson, T. Gorkhover, R. N. Coffee, G. Coslovich, D. Ray, T. Osipov, D. M. Neumark, C. Bostedt, A. F. Vilesov, and O. Gessner, Phys. Rev. Lett. **129**, 073201 (2022).
[18] B. Langbehn *et al.*, New J. Phys. **24**, 113043 (2022).
[19] C. Peltz *et al.*, New J. Phys. **24**, 043024 (2022).
[20] Y. Ihm *et al.*, Nat. Commun. **10**, 2411 (2019).
[21] J. N. Clark, L. Beitra, G. Xiong, D. M. Fritz, H. T. Lemke, D. Zhu, M. Chollet, G. J. Williams, M. M. Messerschmidt, B. Abbey, R. J. Harder, A. M. Korsunsky, J. S. Wark, D. A. Reis, and I. K. Robinson, Proc. Natl. Acad. Sci. U.S.A. **112**, 7444 (2015).
[22] J. N. Clark, L. Beitra, G. Xiong, A. Higginbotham, D. M. Fritz, H. T. Lemke, D. Zhu, M. Chollet, G. J. Williams, M. Messerschmidt, B. Abbey, R. J. Harder, A. M. Korsunsky, J. S. Wark, and I. K. Robinson, Science **341**, 56 (2013).
[23] A. Von Reppert, R. Sarhan, F. Stete, J. Pudell, N. Del Fatti, A. Crut, J. Koetz, F. Liebig, C. Prietzel, and M. Bargheer, J. Phys. Chem. C **120**, 28894 (2016).
[24] C. Jung *et al.*, Sci. Adv. **7**, eabj8552 (2021).
[25] D. Sung, D. Nam, M. Kim, S. Kim, K. S. Kim, S.-Y. Park, S. M. Hwang, C. Jung, H. Lee, D. H. Cho, M. Kim, I. Eom, S. Y. Lee, C. Song, and S. Kim, Appl. Sci. **11**, 5082 (2021).
[26] C. Wu and L. V. Zhigilei, Appl. Phys. A **114**, 11 (2014).
[27] J. Shin, C. Jung, Y. Ihm, S.-P. Heo, D. Nam, S. Kim, M. Kim, I. Eom, J. H. Shim, D. Y. Noh, and C. Song, Nano Lett. **23**, 1481 (2023).
[28] D. Reinhard, B. D. Hall, D. Ugarte, and R. Monot, Phys. Rev. B **55**, 7868 (1997).
[29] I. Barke, H. Hartmann, D. Rupp, L. Flückiger, M. Sauppe, M. Adolph, S. Schorb, C. Bostedt, R. Treusch, C. Peltz, S. Bartling, T. Fennel, K.-H. Meiwes-Broer, and T. Möller, Nat. Commun. **6**, 6187 (2015).
[30] A. Colombo *et al.*, Sci. Adv. **9**, eade5839 (2023).
[31] U. Kreibig and L. Genzel, Surf. Sci. **156**, 678 (1985).
[32] M. A. El-Sayed, Acc. Chem. Res. **34**, 257 (2001).
[33] T. Klar, M. Perner, S. Grosse, G. von Plessen, W. Spirkl, and J. Feldmann, Phys. Rev. Lett. **80**, 4249 (1998).
[34] S. Link, C. Burda, B. Nikoobakht, and M. A. El-Sayed, J. Phys. Chem. B **104**, 6152 (2000).
[35] H. Petrova, C.-H. Lin, S. de Liejer, M. Hu, J. M. McLellan, A. R. Siekkinen, B. J. Wiley, M. Marquez, Y. Xia, J. E. Sader, and G. V. Hartland, J. Chem. Phys. **126**, 094709 (2007).
[36] G. V. Hartland, Chem. Rev. **111**, 3858 (2011).
[37] S. Link and M. A. El-Sayed, Annu. Rev. Phys. Chem. **54**, 331 (2003).
[38] G. V. Hartland, L. V. Besteiro, P. Johns, and A. O. Govorov, ACS Energy Lett. **2**, 1641 (2017).
[39] C. Voisin, N. Del Fatti, D. Christofilos, and F. Vallée, J. Phys. Chem. B **105**, 2264 (2001).
[40] G. Beane, T. Devkota, B. S. Brown, and G. V. Hartland, Rep. Prog. Phys. **82**, 016401 (2018).
[41] D. Hoeing *et al.*, Nano Lett. **23**, 5943 (2023).
[42] W. A. Ackermann, G. Asova, V. Ayvazyan, A. Azima, N. Baboi, J. Bähr, V. Balandin, B. Beutner, A. Brandt, A. Bolzmann *et al.*, Nat. Photonics **1**, 336 (2007).
[43] B. Erk *et al.*, J. Synchrotron Radiat. 25, 1529 (2018).
[44] H. Haberland, M. Karrais, and M. Mall, Z. Phys. D **20**, 413 (1991).
[45] H. Haberland, M. Mall, M. Moseler, Y. Qiang, T. Reiners, and Y. Thurner, J. Vac. Sci. Technol. A **12**, 2925 (1994).
[46] H. Hartmann, V. Popok, I. Barke, V. von Oeynhausen, and K.-H. Meiwes-Broer, Rev. Sci. Instrum. **83**, 073304 (2012).
[47] L. Strüder *et al.*, Nucl. Instrum. Methods Phys. Res. **614**, 483 (2010).
[48] A. Colombo, M. Sauppe, A. A. Haddad, K. Ayyer, M. Babayan, R. Dagar, L. Hecht, G. Knopp, K. Kolatzki, F. Maia *et al.*, arXiv:2409.07413.
[49] R. A. Kirian and H. N. Chapman, Imaging of objects by coherent diffraction of x-ray free-electron laser pulses, in *Synchrotron Light Sources and Free-Electron Lasers* (Springer International Publishing, New York, 2020), pp. 1337–1397.
[50] A. Colombo and D. Rupp, Imaging clusters and their dynamics with single-shot coherent diffraction, in *Structural Dynamics with X-Ray and Electron Scattering* (Royal Society of Chemistry, London, 2023), pp. 172–232.
[51] A. Colombo, D. E. Galli, L. De Caro, F. Scattarella, and E. Carlino, Sci. Rep. **7**, 42236 (2017).
[52] See Supplemental Material at http://link.aps.org/supplemental/10.1103/PhysRevLett.134.136101 for additional figures, videos, and methods, which includes Refs. [30,43,48–51,53–74].

[53] H. W. Sheng, M. J. Kramer, A. Cadien, T. Fujita, and M. W. Chen, Phys. Rev. B **83**, 134118 (2011).
[54] R. Fahdiran and H. M. Urbassek, Eur. Phys. J. D **69**, 35 (2015).
[55] A. P. Thompson, H. M. Aktulga, R. Berger, D. S. Bolintineanu, W. M. Brown, P. S. Crozier, P. J. in 't Veld, A. Kohlmeyer, S. G. Moore, T. D. Nguyen, R. Shan, M. J. Stevens, J. Tranchida, C. Trott, and S. J. Plimpton, Comput. Phys. Commun. **271**, 108171 (2022).
[56] A. H. Larsen *et al.*, J. Phys. Condens. Matter **29**, 273002 (2017).
[57] P. Grigorev, L. Frérot, F. Birks, A. Gola, J. Golebiowski, J. Grießer, J. L. Hörmann, A. Klemenz, G. Moras, W. G. Nöhring, J. A. Oldenstaedt, P. Patel, T. Reichenbach, T. Rocke, L. Shenoy, M. Walter, S. Wengert, L. Zhang, J. R. Kermode, and L. Pastewka, J. Open Source Software **9**, 5668 (2024).
[58] A. Stukowski, Model. Simul. Mater. Sci. Eng. **18**, 015012 (2009).
[59] M. Parrinello and A. Rahman, J. Appl. Phys. **52**, 7182 (1981).
[60] T. F. J. Bögels and R. Caracas, Phys. Rev. B **105**, 064105 (2022).
[61] H. Huang and L. V. Zhigilei, J. Phys. Chem. C **125**, 13413–13432 (2021).
[62] D. S. Ivanov and L. V. Zhigilei, Phys. Rev. B **68**, 064114 (2003).
[63] A. M. Brown, R. Sundararaman, P. Narang, W. A. Goddard, and H. A. Atwater, Phys. Rev. B **94**, 075120 (2016).
[64] Z. Lin, L. V. Zhigilei, and V. Celli, Phys. Rev. B **77**, 075133 (2008).
[65] B. Mahieu, N. Jourdain, K. Ta Phuoc, F. Dorchies, J.-P. Goddet, A. Lifschitz, P. Renaudin, and L. Lecherbourg, Nat. Commun. **9**, 3276 (2018).
[66] A. Ng, Phys. Rep. **1089**, 1 (2024).
[67] Q. L. D. Nguyen, J. Simoni, K. M. Dorney, X. Shi, J. L. Ellis, N. J. Brooks, D. D. Hickstein, A. G. Grennell, S. Yazdi, E. E. B. Campbell, L. Z. Tan, D. Prendergast, J. Daligault, H. C. Kapteyn, and M. M. Murnane, Phys. Rev. Lett. **131**, 085101 (2023).
[68] T. Soddemann, B. Dünweg, and K. Kremer, Phys. Rev. E **68**, 046702 (2003).
[69] R. D. Groot and P. B. Warren, J. Chem. Phys. **107**, 4423 (1997).
[70] A. K. Upadhyay, N. A. Inogamov, B. Rethfeld, and H. M. Urbassek, Phys. Rev. B **78**, 045437 (2008).
[71] A. A. Sorokin, Y. Bican, S. Bonfigt, M. Brachmanski, M. Braune, U. F. Jastrow, A. Gottwald, H. Kaser, M. Richter, and K. Tiedtke, J. Synchrotron Radiat. **26**, 1092 (2019).
[72] J. R. Fienup, Appl. Opt. **21**, 2758 (1982).
[73] S. Marchesini, H. He, H. N. Chapman, S. P. Hau-Riege, A. Noy, M. R. Howells, U. Weierstall, and J. C. H. Spence, Phys. Rev. B **68**, 140101(R) (2003).
[74] S. Marchesini, Rev. Sci. Instrum. **78**, 011301 (2007).
[75] C. Jiang, Y. Mo, H. Wang, R. Li, M. Huang, and S. Jiang, Comput. Mater. Sci. **196**, 110545 (2021).
[76] Y. Gan, H. Cai, and C. Niu, ACS Omega **7**, 39287 (2022).
[77] J. C. Castro-Palacio, K. Ladutenko, A. Prada, G. González-Rubio, P. Díaz-Núñez, A. Guerrero-Martínez, P. Fernández de Córdoba, J. Kohanoff, J. M. Perlado, O. Peña-Rodríguez, and A. Rivera, J. Phys. Chem. Lett. **11**, 5108 (2020).
[78] E. Leveugle, A. Sellinger, J. M. Fitz-Gerald, and L. V. Zhigilei, Phys. Rev. Lett. **98**, 216101 (2007).
[79] L. Delfour and T. E. Itina, J. Phys. Chem. C **119**, 13893–13900 (2015).
[80] G. Paltauf and P. E. Dyer, Chem. Rev. **103**, 487 (2003).
[81] R. Fahdiran, E. Handoko, I. Sugihartono, and H. M. Urbassek, MATEC Web Conf. **197**, 04004 (2018).
[82] W. Haynes, *Handbook of Chemistry and Physics*, 97th Ed. (Boca Raton, CRC Press, FL, 2017).
[83] G. I. Taylor, Proc. R. Soc. A **253**, 313 (1959).
[84] H. Lhuissier and E. Villermaux, J. Fluid Mech. **696**, 5 (2012).
[85] A. Vogel and V. Venugopalan, Chem. Rev. **103**, 577 (2003).
[86] Jülich Supercomputing Centre, JLSRF **7**, A183 (2021).